東北大学機関リポジトリ
TOUR
Tohoku University Repository

Effect of molecular elongation on the thermal conductivity of diatomic liquids

Effect of molecular elongation on the thermal conductivity of diatomic liquids

Takashi Tokumasu,[a] Taku Ohara, and Kenjiro Kamijo
Institute of Fluid Science, Tohoku University, 2-1-1, Katahira, Aoba-ku, Sendai, 980-8577, Japan

The effect of molecular elongation on the thermal conductivity of diatomic liquids has been analyzed using a nonequilibrium molecular dynamics (NEMD) method. The two-center Lennard-Jones model was used to express the intermolecular potential acting on liquid molecules. The simulations were performed using the nondimensional form of the potential so that the molecular elongation, d/σ, was the only parameter varied in the simulation. The simulations were performed for five values of this parameter. First, the equation of state of each liquid was obtained using equilibrium molecular dynamics simulation, and the critical temperature, density, and pressure of each liquid were determined. Then, NEMD simulations of heat conduction in the five liquids were performed using values for temperature and density which were identical among the five liquids when they were reduced by their respective critical temperature and density ($T = 0.7\ T_{cr}$ and $\rho = 2.24\ \rho_{cr}$). Obtained thermal conductivities were reduced by the critical temperature, density, and molecular mass of each compound, and these values were compared with each other. It was found that the reduced thermal conductivity increased as molecular elongation increased. Detailed analysis of the molecular contribution to the thermal conductivity revealed that (a) the contribution of the heat flux caused by energy transport and by translational energy transfer to the thermal conductivity is independent of the molecular elongation, and (b) the contribution of the heat flux caused by rotational energy transfer to the thermal conductivity increases with the increase in the molecular elongation. © *2003 American Institute of Physics.* [DOI: 10.1063/1.1540089]

I. INTRODUCTION

Heat conduction is a basic mechanism which governs thermal phenomena. One of the most important problems in the field of molecular thermophysical engineering is to understand the mechanism of heat conduction at the molecular level. Understanding this mechanism enables us not only to predict macroscopic heat conduction characteristics but also to control the heat conduction in a microscopic system where the macroscopic thermodynamic properties cannot be defined, such as in a nonequilibrium field or on a very small time scale such as in laser heating.

Energy transfer between molecules due to molecular interaction is a dominant factor in heat conduction in liquids, while energy transported via molecular motion governs heat conduction in gases. A number of molecular dynamics (MD) studies on heat conduction in liquids have been reported[1–10] in which the thermal conductivity of pure liquids[1,2,4–7,9,10] and binary mixtures[2,3,8] was examined. These studies employed either equilibrium MD,[1–3] using the Green–Kubo formula, or a nonequilibrium MD (NEMD) (Refs. 4–10) approach, in which a fictitious field was introduced to drive heat flux[4–6] or a real temperature gradient was given to the system by special boundary conditions.[7–10] There was good agreement among these studies, and therefore it can be said

that the basic method to calculate thermal conductivity by MD simulations has been established.

However, most of these studies treat heat conduction in simple Lennard-Jones fluids[1–4,7,8,10] and there has been little research on heat conduction of liquids composed of polyatomic molecules that takes the rotational motion of molecules into consideration. In research to date, the thermal conductivity of liquids such as CO_2 (Refs. 5 and 6) has been calculated considering molecular rotational motion, and the effect of the hydrogen-bond on thermal conductivity in water[9] has been analyzed. However, there have been no reports in which the dependence of molecular shape on heat conduction was analyzed in detail. Such a study would enable us not only to explore the microscale energy transfer of liquids or the heat conduction of a liquid in a nonequilibrium state, but would also make it possible to choose or design liquids having the required thermal conductivity in a certain condition.

In the present paper, the dependence of the thermal conductivity of a diatomic liquid on molecular elongation was analyzed by NEMD simulations. The two-center Lennard-Jones (2CLJ) model was used to express the intermolecular potential acting on liquid molecules. The simulations were performed using the nondimensional form of the potential so that the molecular elongation, d/σ, was the only parameter varied in the simulation. The NEMD simulations were performed for five cases of the parameter, which yielded thermal conductivities of the five simulated liquids. The simula-

[a] Electronic mail: tokumasu@ifs.tohoku.ac.jp; Tel and Fax: +81-22-217-5239.

TABLE I. The parameters for each of the five cases. d/σ, molecular elongation; σ, ε, parameters of Eq. (2); m, mass of a molecule.

	d/σ	σ (Å)	ε/k (K)	m (kg)	Corresponding molecules
Case 1	0.22	3.2104	38.003	5.31×10^{-26}	O_2
Case 2	0.39	3.2717	42.282	4.65×10^{-26}	CO
Case 3	0.59	3.7509	232.26	1.26×10^{-25}	CS_2
Case 4	0.73	3.2618	201.31	1.18×10^{-25}	Cl_2
Case 5	0.98	3.2843	345.47	2.65×10^{-25}	Br_2

tion conditions, when reduced by their respective critical values, were the same for all cases. In the next section, the equation of state (EOS) of each liquid is obtained by MD simulations and the critical density, temperature and pressure are determined for each liquid. In Sec. III, the thermal conductivity of each liquid at the same temperature and density, reduced by their respective critical density and temperature obtained in Sec. II, is determined by NEMD simulations under a real temperature gradient, which agrees with experimental results. The results are discussed in Sec. IV.

II. EQUATION OF STATE AND THE CRITICAL POINT OF EACH LIQUID

In the present paper, the two-center Lennard-Jones (2CLJ) potential[11] described below was used to express an interaction potential between the molecules,

$$\psi_{2CLJ} = \sum_{a=1}^{2} \sum_{b=1}^{2} \psi_{LJ}(r_{ia,jb}), \tag{1}$$

where a and b denote nuclei which belong to molecule i and j, respectively, and $r_{ia,jb}$ denotes the distance between nucleus a of molecule i and nucleus b of molecule j. The symbol, $\psi_{LJ}(r)$, denotes the following Lennard-Jones potential:

$$\psi_{LJ}(r) = 4\varepsilon \left\{ \left(\frac{\sigma}{r} \right)^{12} - \left(\frac{\sigma}{r} \right)^{6} \right\}. \tag{2}$$

The simulations were performed using the nondimensional form of the potential so that only the molecular elongation, d/σ, was varied during the simulation. The simulations were performed for five cases of the parameter as shown in Table I.[12] One-half of the mass of the molecule was assigned to each nucleus. The values in the table correspond to those reported in Ref. 12 for O_2, CO, CS_2, Cl_2, and Br_2. The simulation results for the liquid properties (vapor pressure and second virial coefficient) based on these values are in good agreement with experimental data in the temperature range between T_{tr} and $0.8T_{cr}$,[12] where T_{tr} is the triple point temperature and T_{cr} is the critical temperature. In Table I, k denotes Boltzmann's constant.

The equations of state of the five liquids have been determined by the method established by Kataoka.[13] In this method, the excess Helmholtz free energy A^e (after subtracting the ideal gas term) was expressed as follows:

$$\frac{\beta A^e}{N} = \sum_{n=1}^{5} \sum_{m=-1}^{5} A_{mn} \left(\frac{\rho}{\rho_o} \right)^{n} \left(\frac{\beta}{\beta_o} \right)^{m}, \tag{3}$$

where ρ, N, and β denote density, number of simulated molecules, and $1/kT$, respectively. The coefficients ρ_o and β_o were introduced in order to make the expansion coefficients in Eq. (3), A_{mn}, dimensionless and were chosen to be $\rho_o = m/\sigma^3$ and $\beta_o = 1/\varepsilon$, respectively. Using A^e, the excess internal energy, E_p, is given by

$$\frac{\beta E_p}{N} = \beta \left\{ \frac{\partial}{\partial \beta} \left(\frac{\beta A^e}{N} \right) \right\}_{\rho}, \tag{4}$$

while the pressure, p, is given by

$$\frac{\beta p}{\rho} - 1 = \rho \left\{ \frac{\partial}{\partial \rho} \left(\frac{\beta A^e}{N} \right) \right\}_{\beta}. \tag{5}$$

These values, p and E_p, were obtained at many state points over wide ranges of temperature and density by MD simulations and the expansion coefficients in Eq. (3), A_{mn}, were derived by a least-square fitting of the simulated excess internal energies and pressures. Details of the method are presented below.

The cubic cell used in the simulations contained 864 molecules. The simulations were performed by changing both temperature and density; during each simulation, these values were fixed. The length of the cell was set at $L = (mN/\rho)^{1/3}$. Periodic boundary conditions were applied in all directions. At the initial condition, the molecules were placed in a fcc lattice structure and the velocity vector of molecule i, $\mathbf{v}_i$, was given according to the Boltzmann distribution at temperature T. Molecular rotational motion was described in the molecular coordinate system. In this system, the positions of the two nuclei of a molecule were $(0,0,d/2)$ and $(0,0,-d/2)$, respectively. The rotational energy of molecule i, e_{ri}, was also given according to the Boltzmann distribution at temperature T, and the angular velocity vector of molecule i was $\boldsymbol{\omega}_i = (\sqrt{2e_{ri}/I},0,0)$ in the molecular coordinate system, where $I = 0.25 \, md^2$ denotes the moment of inertia of the molecule. The orientation of the molecule was described by the Euler angle, (ϕ,θ,ψ).[14] The initial Euler angle was given as $\phi_i = 2\pi R$, $\theta_i = \cos^{-1} R$, and $\psi_i = 2\pi R$ by using a random number, R $(0<R<1)$. Integration of the equation of motion was performed by the Verlet algorithm,[14] and the dimensionless time step rescaled by $\sigma\sqrt{m/\varepsilon}$ was $\Delta t^* = 0.0025$. The molecular rotational motion was calculated using quaternions.[15] The cutoff distance for the intermolecular force was $r_c = 3.5 \, \sigma$ and the contributions of molecules which were beyond the cutoff distance to pressure and excess internal energy were corrected by adding a long range correction terms.[11] The MD simulations were performed with temperature control of the system by velocity scaling during the initial 2000 steps to establish a state of equilibrium at temperature T and without temperature control during the next 18 000 steps. The data of the initial 5000 steps were abandoned and those of the next 15 000 steps were analyzed. The temperature, T, pressure, P, and excess internal energy, E_p were determined by

$$T = \frac{2}{5Nk} \sum_{i=1}^{N} \left(\frac{1}{2} m\mathbf{v}_i^2 + \frac{1}{2} \boldsymbol{\omega}_i \cdot \mathcal{I} \cdot \boldsymbol{\omega}_i \right), \tag{6}$$

$$P = \frac{NkT}{V} + \frac{1}{3V}\left[\sum_{i=1}^{N}\sum_{j>i}^{N} \boldsymbol{r}_{ij}\cdot\boldsymbol{F}_{ij}\right]_{r<r_c} + \Delta p, \tag{7}$$

and

$$E_p = \left[\sum_{i=1}^{N}\sum_{j>i}^{N} \psi_{2\mathrm{CLJ}}\right]_{r<r_c} + \Delta E_p, \tag{8}$$

respectively. In the equations, N, V, and $\boldsymbol{r}_{ij}$ denote the number of molecules, the volume of the system, and the vector from the center of mass of molecule j to that of molecule i, respectively. $\mathcal{I}$ denotes the tensor of inertia. The force vector from molecule j to molecule i, $\boldsymbol{F}_{ij}$, is expressed by

$$\boldsymbol{F}_{ij} = \sum_{a=1}^{2}\sum_{b=1}^{2}\left\{-\frac{\partial\psi_{\mathrm{LJ}}(r_{iajb})}{\partial r_{iajb}}\right\}. \tag{9}$$

The expression of the long range correction of pressure, Δp, and that of the excess internal energy, ΔE_p, were obtained based on the assumption that the distribution of LJ centers was uniform beyond the cutoff distance,[11]

$$\Delta p = \frac{64\pi N^2}{3V^2}\varepsilon\sigma^3\left\{\frac{2}{3}\left(\frac{\sigma}{r_c}\right)^9 - \left(\frac{\sigma}{r_c}\right)^3\right\}, \tag{10}$$

$$\Delta E_p = \frac{32\pi N^2}{V}\varepsilon\sigma^3\left\{\frac{1}{9}\left(\frac{\sigma}{r_c}\right)^9 - \frac{1}{3}\left(\frac{\sigma}{r_c}\right)^3\right\}. \tag{11}$$

Dimensionless state quantities described below are introduced for the rest of this paper,

$$\rho^* = \rho\sigma^3/m, \qquad T^* = kT/\varepsilon, \qquad P^* = P\sigma^3/\varepsilon. \tag{12}$$

At first, 160 state points were defined by selecting twenty values of ρ^* ($\rho^* = 0.001, 0.01, 0.05, 0.1, 0.15, 0.2, 0.25, 0.3, 0.35, 0.4, 0.45, 0.5, 0.55, 0.6, 0.65, 0.7, 0.75, 0.8, 0.85, 0.9$) and eight values of T^* ($T^* = 1.5, 2.0, 2.5, 3.0, 3.5, 4.0, 4.5, 5.0$). The selected state points, however, included those where the system was in a two phase state. It is necessary to exclude such state points from those to be examined. It has been reported that in MD simulations the temperature of a system deviates greatly from the target temperature when the state of the system is two-phase.[16] Therefore the data obtained at the state points for which the temperature (averaged over the data acquisition steps) changed more than 5% of the target temperature were regarded as those from two-phase cases, and were excluded from the data set utilized to determine the EOS. On the other hand, it is probable that the system is in a solid state in the high-density and low-temperature regions. It was confirmed that in the low temperature region the mean square displacement of the system during the simulation decreases rapidly from 20σ to 0 when the density exceeds a certain value. In this research, the data with a mean square displacement during the simulation of less than 5σ were regarded to be a those from a solid state case, and were excluded from the determination of the EOS.

Moreover, it is not appropriate to use the MD data in the thermodynamically unstable region because the states in this region are two-phase. It is necessary to obtain the spinodal line to define the unstable region. The spinodal line is a envelope determined by the points where $(\partial p/\partial\rho)_T = 0$ is
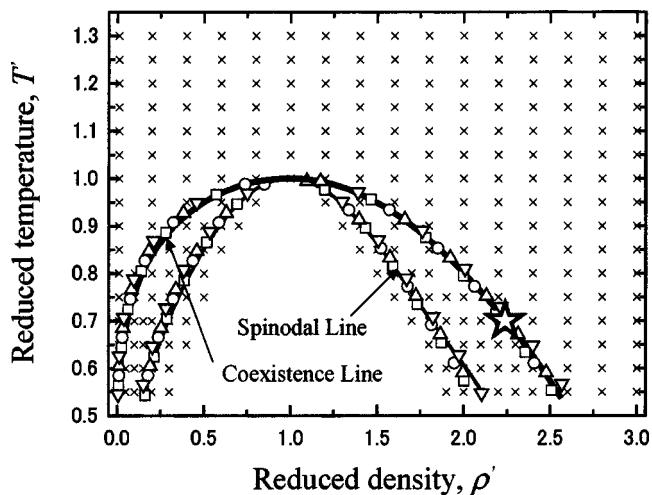

FIG. 1. Simulated state points. ×, simulation points for equation of state. The coexistence and spinodal lines of case 1 are also shown by the thick line and thin line, respectively. Those of case 2 (□), case 3 (○), case 4 (△), and case 5 (▽) are also plotted. star, simulation point for thermal conductivity.

satisfied. In the present work, the EOS was first obtained without excluding the data in the unstable region and the spinodal line was obtained from the EOS by calculating the density where $(\partial p/\partial\rho)_T = 0$ was satisfied at $T^* > 1.5$. Next, the state points in the unstable region enclosed by the spinodal line were excluded and the EOS was calculated using the rest of the data. The spinodal line obtained from the new EOS was different from the old one and this calculation must be an iterative process. The EOS was repeatedly calculated until the results converged.

Using the EOS, a coexistence line was obtained and the critical temperature, density, and pressure were calculated using the following relations:[17]

$$\tfrac{1}{2}(\rho_l + \rho_v) = AT + B, \tag{13}$$

$$\rho_l - \rho_v = C\left(1 - \frac{T}{T_{\mathrm{cr}}}\right), \tag{14}$$

where A, B, and C are constants.

However, there were significant differences among the critical points obtained here for the five liquids and therefore the 160 state points selected above did not necessarily cover the temperature and density ranges required to determine the EOS for these liquids. A second set of 160 state points were selected in the nondimensional space of densities and temperatures which were reduced by the critical density and temperature of each liquid obtained above. Equilibrium MD simulations were performed again and the new pressure and internal energy at the points were obtained. Using these data, new EOSs and critical values were obtained in the same manner. Figure 1 shows a map of the new state points. The critical temperature, T_{cr}^*, density, ρ_{cr}^*, and pressure, P_{cr}^*, are shown in Table II. The dimensional critical values and experimental results are also shown in Table II. The critical values obtained by the EOS of Eq. (3) are slightly different from those obtained by experiment. The reason is that the parameters of Table I are defined so that the liquid properties are in good agreement with experimental results at the range

TABLE II. The dimensionless critical values of each liquid obtained by the EOS of Eq. (3). The left column for each parameter gives dimensionless values; values in the right column are dimensionalized by σ, ε, and m in Table I. P'_{cr} is obtained by Eq. (15). Values in the brackets show the experimental data (Ref. 18).

	T^*_{cr}	T_{cr} (K)	ρ^*_{cr}	ρ_{cr} (kg/m³)	P^*_{cr}	P_{cr} (MPa)	P'_{cr}
Case 1	4.24	161	0.282	452	0.403	6.39	0.337
		(155)		(436)		(5.04)	
Case 2	3.24	137	0.240	318	0.257	4.28	0.331
		(133)		(300)		(3.49)	
Case 3	2.50	580	0.201	482	0.164	9.99	0.327
		(552)		(440)		(7.90)	
Case 4	2.18	437	0.181	613	0.128	10.23	0.326
		(417)		(573)		(7.70)	
Case 5	1.81	626	0.157	1179	0.093	12.48	0.325
		(584)		(1180)		(10.34)	

of temperature between T_{tr} and $0.8T_{cr}$. These results were reduced by their respective critical values and compared with each other. The reduced density, ρ', temperature, T' and pressure, P', were obtained by

$$\rho' = \rho/\rho_{cr}, \quad T' = T/T_{cr}, \quad P' = P/(\rho_{cr}kT_{cr}/m), \quad (15)$$

respectively. The reduced critical pressures, P'_{cr}, are also shown in Table II. As shown in this table, the reduced critical pressure of all liquids agrees well. In the simulation it was found that the reduced equations of state for the liquids also agree well. Reduced spinodal and coexistence lines of all liquids obtained from the EOS are shown in Fig. 1. As shown in this figure, the reduced spinodal and coexistence lines of each liquid agree well regardless of the molecular elongation.

III. THERMAL CONDUCTIVITY OF EACH LIQUID

In order to analyze the effect of molecular elongation on heat conduction, the thermal conductivity of each liquid was evaluated by nonequilibrium MD (NEMD) simulations. Most NEMD studies introduced a fictitious field to drive heat flux by adding special terms to the equation of molecular motion. However, introduction of a fictitious field may not be appropriate for the present study because its influence on the interaction between the molecules is not fully understood. In the present work, therefore, we introduced heat flux by defining a temperature gradient in the system by heating the liquid at one end region of the system and cooling the liquid at the other end region of the system.[10]

The modeled system is shown in Fig. 2. A rectangular cell with a length of $4L$ in the x direction, and L in the y and z directions contained 1728 molecules. The temperature gradient was introduced in the x direction. Periodic boundary conditions were applied in the y and z directions. For each end face of the cell in the x direction, a Lennard-Jones (12-6) potential was applied to all the molecules according to the distance between the molecules and the end face in order to prevent them from passing through the end face.[10] The temperature of the region at each end of the cell in the x direction was controlled by scaling the velocity of all the molecules in the region; the temperature in the region within $L/2$
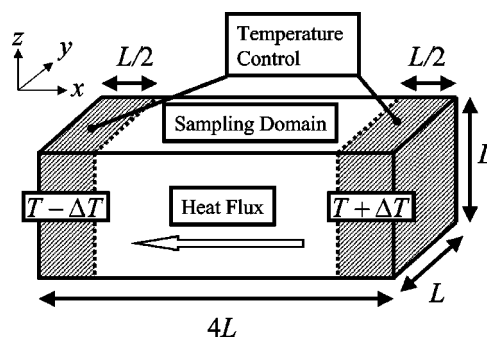

FIG. 2. Domain for the simulation of thermal conductivity.

from one end face in the x direction was kept at $T-\Delta T$, while that in the region within $L/2$ from the other end face was kept at $T+\Delta T$ as shown in Fig. 2. The temperature and density of the liquids were chosen so that these quantities, when reduced by their critical values obtained in Sec. II, were the same. The temperature was $T = 0.7\,T_{cr}$ and the temperature difference was $\Delta T = 0.07\,T_{cr}$. The length of the simulation cell, L, was determined so that the density of the sampling domain (the region of $L/2 < x < 7/2L$) was the saturated density at the temperature of the system. These values are shown in Table III. This state point is shown in Fig. 1. In the simulations, the cutoff distance was $r_c = 4\sigma$ and long range correction of pressure and excess internal energy were not applied. The data from the initial 1 000 000 steps were abandoned and those of the next 2 000 000 steps were analyzed. During the simulation, temperature control was applied to each temperature control region for 10 steps at every 1000 steps.

The heat flux of each liquid, taking into consideration the rotational degree of freedom, $\dot{q}_x$, was obtained by the following equation:[10]

$$\dot{q}_x V = \sum_{i=1}^{\hat{N}} E_i v_{ix} + \frac{1}{2}\sum_{i=1}^{N}\sum_{j \neq i}^{N} \hat{r}_{ijx}(\boldsymbol{v}_i\cdot\boldsymbol{F}_{ij} + \boldsymbol{\omega}_i\cdot\boldsymbol{N}_{ij}), \quad (16)$$

where $V = 3L^3$, N_{ij}, $\hat{N}$, and $\hat{r}_{ijx}$ denote the volume of sampling domain, the torque vector from molecule j to molecule i, the number of molecules in the sampling domain, and the x length of the portion of the distance between molecule i

TABLE III. Dimensionless thermal conductivity obtained by MD simulation and experimental data. L, The length of the simulation domain. For each parameter, the left column gives the dimensionless values, while the right column gives values dimensionalized by σ, ε, and m in Table I. λ' is obtained by Eq. (20). Values in the brackets show the experimental data (Ref. 18).

	L^*	L (nm)	$0.7\,T^*_{cr}$	$0.7\,T_{cr}$ (K)	λ^*	λ (mW/mk)	λ'
Case 1	10.0	3.23	2.97	113	8.75	116	9.88
						(120)	
Case 2	10.6	3.47	2.27	96	8.03	116	11.6
						(115)	
Case 3	11.2	4.22	1.75	406	6.44	101	11.9
Case 4	11.7	3.80	1.52	306	5.83	116	12.4
						(131)	
Case 5	12.2	4.01	1.27	438	4.93	85	12.6
						(90)	

and j contained in the sampling domain, respectively. The total energy of molecule i, E_i, was obtained by

$$E_i = \frac{1}{2} m \boldsymbol{v}_i^2 + \frac{1}{2} \boldsymbol{\omega}_i \cdot \mathcal{I} \cdot \boldsymbol{\omega}_i + \frac{1}{2} \sum_{j=1}^{N} E_{p,ij}, \tag{17}$$

where $E_{p,ij}$ denotes the potential energy between molecule i and j. The thermal conductivity of the liquid, λ, was obtained by the following equation using $\dot{q}_x$ in Eq. (16):

$$\dot{q}_x = -\lambda \frac{\partial T}{\partial x}. \tag{18}$$

The simulation cell was divided into 50 slabs and the temperature of each slab was calculated. The temperature gradient was obtained by approximating the temperature distribution of the simulation cell by a linear function.

In the present simulation, energy, E, heat flux, $\dot{q}$, and thermal conductivity, λ were obtained in their nondimensional forms, which are rescaled by σ, ε, m and reduced by T_{cr}, ρ_{cr}, m in the same manner as ρ, T, and P. The "dimensionless" values are obtained by

$$E^* = E/\varepsilon, \quad \dot{q}^* = \dot{q}/(\varepsilon \sqrt{\varepsilon/m}/\sigma^3),$$
$$\lambda^* = \lambda/(k \sqrt{\varepsilon/m}/\sigma^2), \tag{19}$$

and "reduced" values are obtained by

$$E' = E/kT_{cr}, \quad \dot{q}' = \dot{q}/(\rho_{cr} k T_{cr} \sqrt{kT_{cr}/m}/m),$$
$$\lambda' = \lambda/[k(kT_{cr}/m)^{1/2}(\rho_{cr}/m)^{2/3}]. \tag{20}$$

The dimensionless thermal conductivity λ^* of each liquid obtained by MD simulation is shown in Table III. The dimensional thermal conductivity and experimental results for real liquids[18] are also shown except for the experimental results of CS_2 for which experimental results are not available. As shown in this table, the thermal conductivity of each liquid obtained by MD simulations agrees with the experimental result within $\pm 10\%$. The reduced thermal conductivity, λ', is also shown in Table III. As shown in this table, the reduced thermal conductivity increases with increased molecular elongation, d/σ.

IV. DISCUSSION

There are two different molecular mechanisms responsible for heat flux in liquids, namely, energy transport due to molecular motion and energy transfer due to molecular interaction. These mechanisms correspond to the first and second terms on the right-hand side of Eq. (16), respectively. In the present paper, we call them the "transport term" and the "interaction term," respectively. The heat flux caused by molecular motion consists of three contributions of translational, rotational, and potential energy transport, which correspond to the first, second and third terms in Eq. (17), respectively. The contributions to the heat flux due to translational, rotational and potential energy transport are defined, respectively, by

$$\dot{q}_{tt} = \frac{1}{V} \sum_{i=1}^{\hat{N}} \left(\frac{1}{2} m \boldsymbol{v}_i^2 \right) v_{ix}, \tag{21}$$

TABLE IV. Dimensionless thermal conductivity of each liquid. Values in the brackets are reduced thermal conductivity obtained by Eq. (20). The columns, $\dot{q}_{tt}$, $\dot{q}_{tr}$, $\dot{q}_{tp}$, $\dot{q}_{it}$, and $\dot{q}_{ir}$, show the contribution of the heat flux defined by Eqs. (21)–(25).

	Total	Transport			Interaction	
		$\dot{q}_{tt}$	$\dot{q}_{tr}$	$\dot{q}_{tp}$	$\dot{q}_{it}$	$\dot{q}_{ir}$
Case 1	8.75	0.92	0.24	0.22	6.70	0.67
	(9.88)	(1.04)	(0.27)	(0.25)	(7.57)	(0.76)
Case 2	8.03	0.69	0.33	0.18	5.26	1.58
	(11.58)	(1.00)	(0.47)	(0.26)	(7.58)	(2.27)
Case 3	6.44	0.49	0.24	0.12	3.75	1.85
	(11.87)	(0.89)	(0.44)	(0.23)	(6.91)	(3.41)
Case 4	5.83	0.42	0.22	0.15	3.36	1.68
	(12.38)	(0.90)	(0.47)	(0.32)	(7.13)	(3.57)
Case 5	4.93	0.31	0.18	0.09	2.87	1.47
	(12.56)	(0.80)	(0.46)	(0.24)	(7.31)	(3.75)

$$\dot{q}_{tr} = \frac{1}{V} \sum_{i=1}^{\hat{N}} \left(\frac{1}{2} \boldsymbol{\omega}_i \cdot \mathcal{I} \cdot \boldsymbol{\omega}_i \right) v_{ix}, \tag{22}$$

and

$$\dot{q}_{tp} = \frac{1}{V} \sum_{i=1}^{\hat{N}} \left(\frac{1}{2} \sum_{j=1}^{N} E_{p,ij} \right) v_{ix}. \tag{23}$$

The heat flux caused by molecular interaction consists of two contributions of translational and rotational energy transfer, which correspond to the first and second terms in the interaction term in Eq. (16). The heat flux caused by translational and rotational energy transfer was defined by

$$\dot{q}_{it} = \frac{1}{2V} \sum_{i=1}^{N} \sum_{i \neq j} \hat{r}_{ijx} (\boldsymbol{v}_i \cdot \boldsymbol{F}_{ij}), \tag{24}$$

and

$$\dot{q}_{ir} = \frac{1}{2V} \sum_{i=1}^{N} \sum_{i \neq j} \hat{r}_{ijx} (\boldsymbol{\omega}_i \cdot \boldsymbol{N}_{ij}), \tag{25}$$

respectively. In order to analyze the correlation between the thermal conductivity of a liquid and molecular elongation, the heat flux was decomposed into the above-mentioned contributions, and a partial thermal conductivity due to each mechanism was obtained by its respective heat flux. The dimensionless and reduced partial thermal conductivities are shown in Table IV and Fig. 3. In the table, the thermal conductivity caused by energy transport is displayed in the "Transport" column and that caused by energy transfer is displayed in the "Interaction" column. The values in the brackets in Table IV show the reduced thermal conductivity λ' obtained by Eq. (20). As shown in Table IV and Fig. 3, while the contribution of energy transport, $\dot{q}_{tt}$, $\dot{q}_{tr}$, and $\dot{q}_{tp}$, and of translational energy transfer, $\dot{q}_{it}$, to the reduced thermal conductivity are almost independent of the molecular elongation, only the contribution of rotational energy transfer, $\dot{q}_{ir}$, to the reduced thermal conductivity increases with the increase in the molecular elongation. Based on these findings, it was concluded that the contribution of rotational
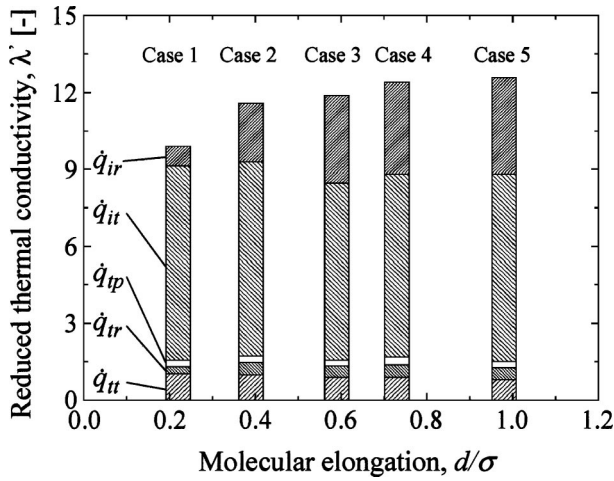
FIG. 3. Contribution of each mechanism to reduced thermal conductivity. The symbols, $\dot{q}_{tt}$, $\dot{q}_{tr}$, $\dot{q}_{tp}$, $\dot{q}_{it}$, and $\dot{q}_{ir}$ denote the contribution of partial heat flux defined by Eqs. (21)–(25), respectively.

TABLE V. Dimensionless virial [the second term on the right-hand side of Eq. (7)] of each liquid. The values in the brackets in Table V show the virial reduced by $\rho k T_{cr}/m$.

	Case 1	Case 2	Case 3	Case 4	Case 5
Virial	−0.81	−0.53	−0.36	−0.30	−0.23
	(−0.68)	(−0.69)	(−0.73)	(−0.77)	(−0.81)

energy transfer to the reduced thermal conductivity is the main cause of the increase in reduced thermal conductivity that is shown in Table III.

As mentioned above, liquid molecules transport energy by molecular motion and transfer their energy to other molecules by molecular interaction. The heat flux caused by molecular motion is expressed by

$$\dot{q}_t = \frac{1}{V}\sum_{i=1}^{\hat{N}}\left(\frac{1}{2}mv_i^2 + \frac{1}{2}\boldsymbol{\omega}_i\cdot\mathcal{I}\cdot\boldsymbol{\omega}_i + \frac{1}{2}\sum_{j=1}^{N}E_{p,ij}\right)v_{ix}. \quad (26)$$

Considering both the equipartition law of energy and the fact that the temperature of each liquid is $T = 0.7\,T_{cr}$, the following equations are obtained:

$$\sum_{i=1}^{\hat{N}}\frac{1}{2}mv_i^2 = 1.5\hat{N}kT = 1.05\hat{N}kT_{cr}, \quad (27)$$

$$\sum_{i=1}^{\hat{N}}\frac{1}{2}\boldsymbol{\omega}_i\cdot\mathcal{I}\cdot\boldsymbol{\omega}_i = \hat{N}kT = 0.7\hat{N}kT_{cr}. \quad (28)$$

Thus the averaged translational and rotational energy of a molecule reduced by kT_{cr} are 1.05 and 0.7, respectively and they are equal among the five liquids regardless of the molecular elongation. Since the reduced EOSs are equal among the five liquids as mentioned in Sec. II, it follows that the excess internal energy reduced by kT_{cr} is equal among the five liquids and therefore the total energy of molecules reduced by kT_{cr} is equal among the five liquids. The probability distribution function of the velocity of molecules in the x direction is given by

$$f_x(v_x)dv_x = \sqrt{\frac{m}{2\pi kT}}\exp\left(-\frac{mv_x^2}{2kT}\right)dv_x. \quad (29)$$

Considering that $T = 0.7T_{cr}$ and the reduced velocity v_x' is given by $v_x' = v_x/\sqrt{kT_{cr}/m}$, the probability distribution function of the reduced velocity is obtained by

$$f_x(v_x')dv_x' = \sqrt{\frac{1}{1.4\pi}}\exp\left\{-\frac{1}{1.4}(v_x')^2\right\}dv_x', \quad (30)$$

and therefore the shape of the distribution function of reduced velocity for all the liquids is the same. Thus, it can be understood that the heat flux in each liquid caused by molecular motion has the same value for all the liquids when reduced by ρ_{cr}, T_{cr}, and m.

The amount of heat flux caused by energy transfer due to molecular interaction is determined by the intermolecular force and torque, and so depends on the probability distribution of intermolecular force and torque. The probability distribution of intermolecular force and torque in the equilibrium state in all the liquids were compared with each other. The number of simulated molecules was $N = 6912$. The state was the same as the simulation of heat conduction in Sec. III ($T = 0.7\,T_{cr}$ and $\rho = 2.24\,\rho_{cr}$). A cubic cell was used and periodic boundary conditions were applied in all directions. The temperature control and data sampling were performed in the same manner as described in Sec. II. In this simulation, the cutoff distance was $r_c = 4\sigma$ and long range correction of the pressure and excess internal energy were not applied.

The virial [the second term on the right-hand side of Eq. (7)], W^*, obtained for each liquid is shown in Table V. The values in the brackets in Table V show the virial reduced by $\rho_{cr}kT_{cr}/m$. As shown in this table, the reduced virial decreases with the increase in the molecular elongation, but the reduction is within a range of 20%. It has been reported that the reduced density, ρ', temperature T', and pressure, P' of a liquid consisting of molecules with a very simple structure obey the same equation of state by the principle of corresponding state.[19–21] These results show this tendency. The virial of each liquid, W, is expressed by the following equation:

$$W = \frac{1}{3V}\sum_{i=1}^{N}\sum_{j>i}^{N}\boldsymbol{r}_{ij}\cdot\boldsymbol{F}_{ij} = \frac{1}{3V}\sum_{i=1}^{N}\sum_{j>i}^{N}\sum_{\alpha=x,y,z}r_{ij\alpha}F_{ij\alpha}$$

$$= \frac{1}{3V}\sum_{i=1}^{N}\sum_{j>i}^{N}\sum_{\alpha=x,y,z}f_{ij\alpha\alpha}|r_{ij\alpha}|, \quad (31)$$

where

$$f_{ij\alpha\beta} = n_{ij\alpha}F_{ij\beta}, \quad (32)$$

and

$$n_{ij\alpha} = \begin{cases} 1 & (r_{ij\alpha} > 0), \\ 0 & (r_{ij\alpha} = 0), \\ -1 & (r_{ij\alpha} < 0). \end{cases} \quad (33)$$

The symbol, $f_{ij\alpha\beta}$, denotes the contribution of intermolecular forces between molecule i and j to the stress in the $\beta(x,y,z)$ direction acting on a surface normal to the $\alpha(x,y,z)$ direction, and at $\alpha = \beta$ it expresses the amount of intermolecular force for which the positive value means re-
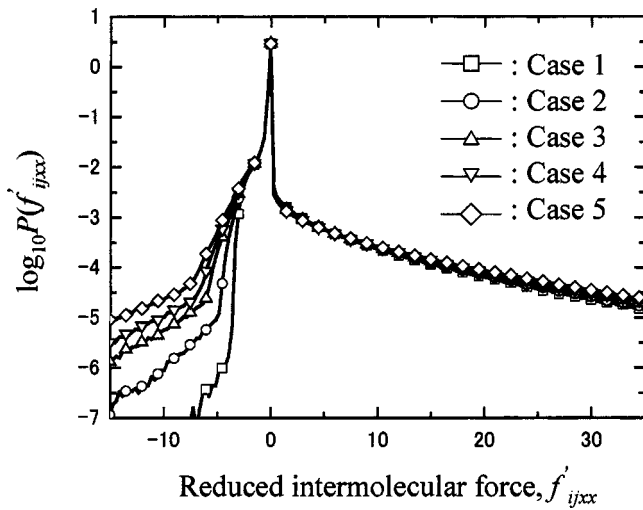
FIG. 4. Probability distribution of reduced intermolecular force, $P(f'_{ijxx})$. $P(f'_{ijxx})$ is defined by Eq. (35).

pulsive force. Using $f_{ij\alpha\beta}$, the heat flux caused by translational energy transfer due to molecular interaction, $\dot{q}_{it}$, is expressed by the following equation:

$$\dot{q}_{it} = \frac{1}{2} \sum_{i=1}^{N} \sum_{j \neq i} \hat{r}_{ijx}(\boldsymbol{v}_i \cdot \boldsymbol{F}_{ij})$$

$$= \sum_{i=1}^{N} \sum_{j>i} \sum_{\alpha=x,y,z} |\hat{r}_{ijx}|(v_{ij\alpha}f_{ijx\alpha}), \qquad (34)$$

where $v_{ij\alpha}$ denotes the average velocity of molecule i and j in the α direction. As shown in Eq. (34), $\dot{q}_{it}$ depends greatly upon the probability distribution of intermolecular force, $f_{ijx\alpha}$. In this simulation the probability distribution of intermolecular force, $P(f'_{ijxx})$, was examined. The reduced intermolecular force was obtained by $f'_{ijxx} = f_{ijxx} / [kT_{cr}(\rho_{cr}/m)^{1/3}]$. $P(f'_{ijxx})$ was determined by summing the occurrence of intermolecular force between f'_{ijxx} and $f'_{ijxx} + df'_{ijxx}$ as

$$P(f'_{ijxx})df'_{ijxx} = \frac{N(f'_{ijxx})}{N_{tot}}, \qquad (35)$$

where $N(f'_{ijxx})$ denotes the integrated total number of intermolecular forces between f'_{ijxx} and $f'_{ijxx} + df'_{ijxx}$. In Eq. (35) N_{tot} was obtained by

$$N_{tot} = \sum_{f'_{ijxx} = -\infty}^{\infty} N(f'_{ijxx}). \qquad (36)$$

In this simulation df'_{ijxx} is 0.25. The probability distribution in Eq. (35) was obtained by counting the intermolecular forces between molecules whose reduced distance, $r'_{ij} = r_{ij}/(m/\rho_{cr})^{1/3}$, is shorter than 2. This enables us to compare the distributions among all the liquids. Figure 4 shows the log plot of the probability distribution of intermolecular force, $P(f'_{ijxx})$, for each liquid. It can be seen in the figure that the probability distribution of the reduced intermolecular force in each liquid in the range of $f'_{ijxx} < -2$ changes greatly according to the molecular elongation, but that the

probability distributions in the range of $f'_{ijxx} > -2$ agree well with each other regardless of the molecular elongation. It can be said that the heat flux is determined by f'_{ijxx} in the range of $f'_{ijxx} > 0$ because both the absolute value and the probability of intermolecular force in the range of $f'_{ijxx} < -2$ are smaller than those in the range of $f'_{ijxx} > 0$. As shown in Eq. (34), the heat flux caused by the translational energy transfer is determined by both the probability distribution of intermolecular force and the probability distribution of molecular velocities. As shown in Fig. 4, the probability distribution of intermolecular force at the same reduced state agrees well in the range of $f'_{ijxx} > 0$, which is the main contributor to the heat flux, regardless of the molecular elongation. Moreover, the probability distributions of the reduced molecular velocity for each liquid agree well with each other, as mentioned above. For this reason, it is considered that the heat fluxes caused by translational energy transfer in each liquid agree well with each other.

The heat flux caused by rotational energy transfer, $\dot{q}_{ir}$, was expressed by the following equation in the same manner:

$$\dot{q}_{ir} = \frac{1}{2} \sum_{i=1}^{N} \sum_{j \neq i} \hat{r}_{ijx}(\boldsymbol{\omega}_i \cdot \boldsymbol{N}_{ij})$$

$$= \frac{1}{2} \sum_{i=1}^{N} \sum_{j>i} \sum_{\alpha=x,y,z} |\hat{r}_{ijx}|(\omega_{i\alpha}T_{ijx\alpha} - \omega_{j\alpha}T_{jix\alpha}), \qquad (37)$$

where the torque acting from molecule j on molecule i was estimated by

$$T_{ij\alpha\beta} = n_{ij\alpha}N_{ij\beta}. \qquad (38)$$

Although this value has no physical meaning, it is useful to examine T_{ijxx} to study $\dot{q}_{ir}$ in the same manner as $\dot{q}_{it}$ in Eq. (34). The probability distribution of reduced torque between molecules, $P(T'_{ijxx})$, was also examined. The reduced torque between molecules, T'_{ijxx}, was obtained by $T'_{ijxx} = T_{ijxx}/kT_{cr}$. $P(T'_{ijxx})$ was defined in the same manner as

$$P(T'_{ijxx})dT'_{ijxx} = \frac{N(T'_{ijxx})}{N_{tot}}, \qquad (39)$$

where $N(T'_{ijxx})$ denotes the integrated total number of torque between molecules between T'_{ijxx} and $T'_{ijxx} + dT'_{ijxx}$. In Eq. (39) N_{tot} was obtained by

$$N_{tot} = \sum_{T'_{ijxx} = -\infty}^{\infty} N(T'_{ijxx}). \qquad (40)$$

In this simulation the reduced dT'_{ijxx} is 0.25. Figure 5 shows the log plot of $P(T'_{ijxx})$ of each liquid. This figure shows that the probability distribution of reduced torque between molecules greatly depends upon the molecular elongation except near $T'_{ijxx} = 0$ and that the probability of larger torque increases with the increase in the molecular elongation. The contribution of the torque between molecules near $T'_{ijxx} = 0$ to the heat flux is small due to the small absolute value, although the probability is large. It is considered that the heat flux caused by rotational energy transfer is determined by the torque between molecules having large absolute value. As
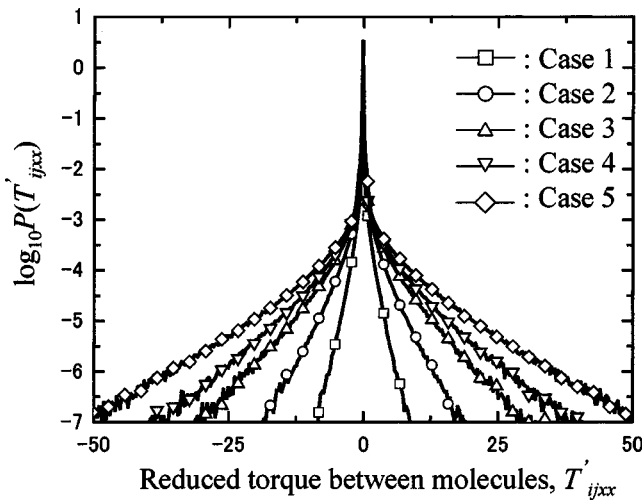
FIG. 5. Probability distribution of reduced torque between molecules, $P(T'_{ijxx})$. $P(T'_{ijxx})$ is defined by Eq. (39).

TABLE VI. Contribution of energy component according to each direction to heat flux (in the case of case 1). These values are obtained by $\dot{q}_{it,p}/\dot{q}_{it}$, $\dot{q}_{it,n}/\dot{q}_{it}$, $\dot{q}_{ir,p}/\dot{q}_{ir}$, and $\dot{q}_{ir,n}/\dot{q}_{ir}$, respectively. The values, $\dot{q}_{it,p}$, $\dot{q}_{it,n}$, $\dot{q}_{ir,p}$, and $\dot{q}_{ir,n}$ are obtained by Eqs. (41)–(44), respectively, and $\dot{q}_{it}$ and $\dot{q}_{ir}$ are obtained by Eqs. (24) and (25), respectively.

	Parallel	Normal
$\dot{q}_{it}$	63.4%	36.6%
$\dot{q}_{ir}$	17.7%	82.3%

shown in Eq. (37), the heat flux caused by the rotational energy transfer is determined by both the probability distribution of the torque between molecules and the probability distribution of the angular velocity of the molecule. As shown in Fig. 5, the probability distribution of the torque between molecules in each liquid differs depending on the molecular elongation although the reduced state of each liquid is the same. Moreover, the probability distribution of the angular velocity of the molecule in each liquid also differs according to the molecular elongation. For this reason, these two differences cause the heat flux due to rotational energy transfer to depend on the molecular elongation.

The contribution of the transfer of energy component according to each direction to the heat flux were analyzed in detail. In the case of translational energy transfer, the contribution of energy component according to the direction ''parallel'' and ''normal'' to the heat flux were obtained by

$$\dot{q}_{it,p}=\frac{1}{2}\sum_{i=1}^{N}\sum_{i\neq j}\hat{r}_{ijx}v_{ix}F_{ijx}, \qquad (41)$$

and

$$\dot{q}_{it,n}=\frac{1}{2}\sum_{i=1}^{N}\sum_{i\neq j}\hat{r}_{ijx}(v_{iy}F_{ijy}+v_{iz}F_{ijz}), \qquad (42)$$

respectively. In the case of rotational energy transfer, they were obtained by

$$\dot{q}_{ir,p}=\frac{1}{2}\sum_{i=1}^{N}\sum_{i\neq j}\hat{r}_{ijx}\omega_{ix}N_{ijx}, \qquad (43)$$

and

$$\dot{q}_{ir,n}=\frac{1}{2}\sum_{i=1}^{N}\sum_{i\neq j}\hat{r}_{ijx}(\omega_{iy}N_{ijy}+\omega_{iz}N_{ijz}), \qquad (44)$$

respectively. Table VI shows the rate of the contribution of energy component according to each direction to the heat flux obtained by Eqs. (41)–(44). In Table VI only the values of case 1 are shown. This table shows that the translational energy transfer is mainly contributed by $\dot{q}_{it,p}$ while the rota-

tional energy transfer is mainly contributed by $\dot{q}_{ir,n}$. The energy transfer in the other cases mentioned in Table I are of the same magnitude. It is therefore predicted that the degree of change of thermal conductivity due to molecular elongation differs under conditions in which the energy excitement in a specific direction is constrained, for instance, as in case of heat conduction near the wall.

V. CONCLUSION

Heat conduction in liquids was studied by MD simulation and the effect of the molecular elongation on thermal conductivity of liquids was analyzed. The two-center Lennard-Jones (2CLJ) model was used to express the intermolecular potential acting on liquid molecules. The simulations were performed using the nondimensional form of the potential so that only the molecular elongation, d/σ, was the simulation parameter. The simulations were performed for five cases of the parameter. Pressure and excess internal energy of each liquid at many state points were first simulated, and equation of state (EOS) and the critical temperature, density, and pressure of each liquid were obtained. Next, thermal conductivity of each liquid at the same temperature and density reduced by these critical values was estimated by nonequilibrium MD (NEMD) simulations. The simulated results agree with the experimental data within 10%. The thermal conductivity reduced by critical density, ρ_{cr}, critical temperature, T_{cr}, and molecular mass, m, increased with the increase in the molecular elongation, d/σ. To investigate the cause of this tendency, the heat flux was decomposed into its component mechanisms, and the contributions of these mechanisms to heat flux were compared. Consequently, while the contributions to the thermal conductivity due to energy transport and translational energy transfer were found to have the same value regardless of the molecular elongation, the contribution to the thermal conductivity due to rotational energy transfer was found to increase with an increase in the molecular elongation. It was also found that the translational energy transfer is mainly contributed by the energy component according to the direction parallel to the heat flux, while the rotational energy transfer is mainly contributed by those normal to the heat flux.

[1] R. Vogelsang, C. Hoheisel, and G. Cicotti, J. Chem. Phys. **86**, 6371 (1987).

[2] P. J. Gardner, D. M. Heyes, and S. R. Preston, Mol. Phys. **73**, 141 (1991).

[3] R. Vogelsang, C. Hoheisel, G. V. Paolini, and G. Cicotti, Phys. Rev. A **36**, 3964 (1987).

[4] G. V. Paolini, G. Cicotti, and C. Massobrio, Phys. Rev. A **34**, 1355 (1986).

[5] D. J. Evans and S. Murad, Mol. Phys. **68**, 1219 (1989).

[6] B. Y. Wang, P. T. Cummings, and D. J. Evans, Mol. Phys. **75**, 1345 (1992).

[7] T. Ikeshoji and B. Hafskjold, Mol. Phys. **81**, 251 (1994).

[8] B. Hafskjold, T. Ikeshoji, and S. K. Ratkje, Mol. Phys. **80**, 1389 (1993).

[9] T. Ohara, J. Chem. Phys. **111**, 6492 (1999).

[10] T. Ohara, J. Chem. Phys. **111**, 9667 (1999).

[11] K. Singer, A. Taylor, and J. V. L. Singer, Mol. Phys. **33**, 1757 (1977).

[12] M. Bohn, R. Lustig, and J. Fischer, Fluid Phase Equilib. **25**, 251 (1986).

[13] Y. Kataoka, J. Chem. Phys. **87**, 589 (1987).

[14] M. P. Allen and D. J. Tildesley, *Computer Simulation of Liquids* (Clarendon, Oxford, 1986).

[15] D. J. Evans, Mol. Phys. **34**, 1317 (1977).

[16] T. Kinjo and M. Matsumoto, Fluid Phase Equilib. **144**, 343 (1998).

[17] E. A. Guggenheim, J. Chem. Phys. **13**, 253 (1945).

[18] *JSME Data Book: Thermophysical Properties of Fluids* (Japan Society of Mechanical Engineering, Tokyo, 1983).

[19] P. A. Monson, Mol. Phys. **53**, 1209 (1984).

[20] D. B. McGuigan, M. Lupkowski, D. M. Pacquet, and P. A. Monson, Mol. Phys. **67**, 33 (1989).

[21] J. Fisher, R. Lustig, H. Breitenfelder-Manske, and W. Lemming, Mol. Phys. **52**, 485 (1984).